*Earth Planets Space*, **53**, 645–653, 2001

# The onset of magnetic reconnection in the magnetotail

Michael Hesse[1] and Karl Schindler[2]

[1]*Electrodynamics Branch, NASA Goddard Space Flight Center, Greenbelt, Maryland, U.S.A.*
[2]*Ruhr-Universität Bochum, Germany*

(Received September 27, 2000; Revised January 9, 2001; Accepted January 15, 2001)

This paper addresses the onset of collisionless magnetic reconnection in the tail of the Earth's magnetosphere. The two-and-a-half-dimensional version of a fully electromagnetic particle-in-cell code is used to describe the pre- and post-onset dynamics of reconnection in thin current sheets in the magnetotail. The ion/electron mass ratio is set to 100. The simulation starts out from an apparently stable equilibrium configuration. Applying an external electric field, meant to be caused by magnetic flux transfer to the tail, leads to the formation of a thin current sheet in the center of the plasma sheet. This confirms earlier results obtains with fluid and hybrid-methods. In the thin sheet quasi-static force-balance leads to a substantial decrease of the north-south component of the magnetic field in the center of the sheet. This in turn causes the electrons to become significantly nongyrotropic, such that a tearing mode starts growing. Regarding the nonideal process that supports the electric field in the diffusion region, the simulation results are shown to be consistent with the notion that electron pressure anisotropies associated with the nongyrotropy generate the required diffusive electric fields. The destabilizing role of electron nongyrotropy is confirmed by a simplified analysis of the energy principle for two-dimensional collisionless plasmas.

## 1. Introduction

Magnetic reconnection is recognized to be one of the most important transport and energy conversion processes in space- and astrophysical plasmas. Magnetic reconnection is a likely contributor to the formation and ejection of coronal mass ejecta (e.g., Gosling *et al.*, 1995; Antiochos *et al.*, 1999) and to coronal heating (e.g., Priest, 1984; Cargill and Klimchuk, 1997), and facilitates the entry of solar wind plasma and electromagnetic energy into the magnetosphere by either low- or high-latitude magnetopause reconnection (e.g., Paschmann *et al.*, 1979; Sonnerup *et al.*, 1981). Inside the magnetosphere, magnetic reconnection converts energy stored mainly in the magnetotail lobes to plasma internal and kinetic energy. Some authors have suggested that magnetic reconnection plays a role in the formation of the auroral acceleration region (Atkinson, 1978; Haerendel, 1987). Thus magnetic reconnection constitutes a critical element in the dynamics of space plasmas throughout the solar system.

Magnetic reconnection requires the presence of a diffusion region, where collisionless or collisional plasma processes facilitate changes in magnetic connection between plasma elements through the generation of dissipative electric fields. Necessarily, this diffusion region is very localized in collisionless plasmas, extending at most to typical ion Larmor radii. Indirect reconnection signatures (contrasted with direct observations of the diffusion region) include the presence of fast flows and plasma heating and particle acceleration associated with magnetic field signatures. Such indirect signatures are observed remotely in the solar corona (e.g., Brueckner, 1996), in the solar wind by the magnetic topology of CMEs, and by direct spacecraft observations at the magnetopause and in the magnetotail of the Earth.

Because of the small scales involved in ion and particularly electron demagnetization, the properties of the diffusion region have not been clearly identified in spacecraft observations. This lack of direct observations is due to two effects. First, the localization of the diffusion region and of the processes acting therein requires spacecraft at appropriate locations with fast plasma instrumentation, which was not available in the past. Second, and more importantly, the physics of the dissipation region remained a mystery until very recently. Therefore, with little theoretical knowledge of what data signatures are to be expected on such an encounter, it is perhaps not surprising that the search for the diffusion region remains on today.

Recent theoretical and modeling efforts, however, have made great strides toward understanding and more comprehensively describing the inner workings of magnetic reconnection in collisionless plasmas, such as dominate in the space regions accessible to direct measurements (Vasyliunas, 1975). Beyond results pertaining to larger scales (e.g., Krauss-Varban and Omidi, 1995; Lin and Swift, 1996; Lottermoser *et al.*, 1998), we now know that electron physical processes relying on the inertia of individual electrons, expressed as either pressure tensor, or bulk inertia effects, are required to facilitate the evolution of the large scale system. Previous analyses of time-dependent magnetic reconnection (Hewett *et al.*, 1988; Pritchett, 1994; Tanaka, 1995a, b; Hesse *et al.*, 1995; Kuznetsova *et al.*, 1998; Hesse and Winske, 1998; Shay *et al.*, 1998a, b; Horiuchi and Sato, 1994, 1997; Cai and Lee, 1997; Hesse *et al.*, 1999; Pritchett, 1994, Birn *et al.*, 2000) have therefore begun to shed light

on the electron behavior in different parameter regimes, primarily in the regions of low magnetic field. Here it was found that, for current sheets of ion inertial length thickness or smaller, deviations from gyrotropy in the electron distribution function can give rise to reconnection electric fields via nongyrotropic electron pressures

$$E_y = -\frac{1}{n_e e}\left(\frac{\partial P_{xye}}{\partial x} + \frac{\partial P_{yze}}{\partial z}\right). \qquad (1)$$

Here the $y$ coordinate is aligned with the main current direction, and $x$ and $z$ are perpendicular. This process can be understood as an inertial effect of thermal electrons which bounce in the field reversal region. For current sheets of reduced thicknesses, down to the collisionless skin depth $c/\omega_e$, bulk electron inertial effects might become important and might generate very fast reconnection rates, albeit for very short times.

It appears self-evident from above that significant reconnection electric fields can result only if large enough nongyrotropic electron pressures of the kind found in Eq. (1) can be found. The gyrotropy brought about by magnetization of electrons in the magnetic field component perpendicular to the magnetotail current sheet is related to the stability of the collisionless tearing mode in the quiet-time magnetotail e.g., Kuznetsova *et al.*, 1995). Recent investigations, however, have suggested that this stabilization might be overcome in the presence of a thin enough current sheet, such as commonly observed just prior to substorm onset. This idea was followed further by Hesse and Birn (2000), who used a kinetic model to simulate thin current sheet formation and the onset of magnetic reconnection in a magnetotail-like configuration. In this paper, we will extend this investigation to a thicker initial current sheet, with a larger magnetic normal component. We will show that the formation of a thin current sheet can overcome the stabilization of collisionless tearing and, thus, of magnetic reconnection even in this configuration.

## 2. The Onset of Magnetic Reconnection in Current Sheets with Finite Magnetic Normal Component

Investigations of the inner workings of magnetic reconnection are naturally much more complicated than studies of the large-scale behavior. In order to understand how ions and electrons become unmagnetized such that their magnetic connection can be changed (see Subsections 2.3 and 3), single particle properties of the plasma have to be properly accounted for. Naturally, this mandates a modeling approach beyond the magnetofluid methods which have been so successfully applied to larger scale problems. The complexity of the particle methods required to study the basic mechanism of magnetic reconnection, however, restricts modeling to simpler geometries, usually, as in our case, to planar models, within which magnetic reconnection relies on the classical X point geometry.

Recently, the modes of operation of magnetic reconnection once the X point has formed were the subject of a number of investigations based on kinetic methods. Rather than reviewing these in great detail, we refer to the literature (e.g., Hewett *et al.*, 1988; Pritchett, 1994; Tanaka, 1995a, b; Hesse *et al.*, 1995; Kuznetsova *et al.*, 1998; Hesse and Winske, 1998; Shay *et al.*, 1998a, b; Horiuchi and Sato, 1994, 1997; Cai and Lee, 1997; Hesse *et al.*, 1999; Pritchett, 1994) for these studies and present here only a brief summary of the pertinent results in Subsection 2.1. Instead, we will present in more detail some new results addressing a contentious issue related to magnetic reconnection: the problem of onset of reconnection in magnetic field configurations mimiking the pre-onset nightside magnetosphere. This study will be the subject of Subsection 2.2.

In the general scenario where the onset of reconnection is due to an instability of a current sheet, the presence of a normal magnetic field component implies that the sheet must become unstable *before* the X-line forms. In fact, the X-line formation is part of the nonlinear regime of the instability. Thus, one is faced with the problem of stability in tail-like fields without neutral points. This problem can be addressed by using a variational technique. In Section 3 we will briefly describe a new result of this approach, which complements the simulation findings.

### 2.1 Basic structure of the reconnection region

Our present understanding of the magnetic reconnection process can be summed up as follows: The diffusion region proper consists of two embedded regions of different physical parameters and sizes. The larger, called the "Hall-Zone" exhibits typical dimensions of a few ion inertial lengths, which in many cases is roughly equivalent to ion Larmor radii in the adjacent high magnetic field regions. In typical magnetospheric plasmas this corresponds to several hundreds of kilometers. Here the larger ion mass generates a region where the ion dynamics decouples from the electrons. The electrons exhibit much faster flow velocities away from the central region than the ions. The resulting currents are consistent with a quadrupolar out-of-plane magnetic field structure roughly aligned with the separatrices. The inner diffusion region is dominated by electron physical processes, which generate the actual reconnection electric field. This electric field can be generated by bulk acceleration in the direction antiparallel to the main current flow, or by electron pressure gradients in the current direction, or by nongyrotropic electron pressure anisotropies (Vasyliunas, 1975; Hesse and Winske, 1997; Kuznetsova *et al.*, 1998). These signatures occur on spatial scales below the ion inertial length, but typically above the collisionless skin depth (of some tens of kilometers).

### 2.2 Numerical approach and initial conditions

For the purpose of the present investigation, we use a two-and-a-half-dimensional version of a our fully electromagnetic particle-in-cell code. The scheme is based on the Buneman layout of currents and fields on a rectangular grid (e.g., Villasenor and Buneman, 1992). Particles are advanced by a second-order, implicit leapfrog algorithm. Densities and fluxes are accumulated on the grid, using a rectangular particle shape function. Charge conservation is guaranteed by the iterative application of a Langdon-Marder-type (Langdon, 1992) correction to the electric field. The electromagnetic fields are integrated implicitly to avoid the Courant constraint on the propagation of light waves. The light wave damping in the implicit scheme also allows us to use simple reflecting boundary conditions for the elec-

tromagnetic fields at the boundaries.

Ions are assumed to be protons (with mass $m_p$) in the following investigations. Further, we normalize lengths to the ion inertial lengths $c/\omega_i = c(e^2 n_0/\epsilon_0 m_p)^{-1/2}$ using a current sheet density $n_0$, and times are normalized to the inverse of the ion cyclotron frequency $\Omega_i = eB_0/m_i$ in the asymptotic magnetic field $B_0$ unless noted otherwise. The magnetic field is normalized to the asymptotic value $B_0$ for large $z$ at $x = 0$. Velocities are normalized to the Alfvén speed $v_A = B_0/\sqrt{\mu_o m_p n_0}$. Consequently, current densities and electric fields are normalized to $j_0 = B_0/(\mu_0 c/\omega_i)$ and $E_0 = v_A B_0$, respectively. In the present calculations, the system dimensions are $L_x = 60c/\omega_i$ and $L_z = 20c/\omega_i$ with $600 \times 300$ cells in $x$, and $z$ directions respectively. Clearly, this simulation box size is considerably smaller than the actual magnetotail. This smaller size is, at present, unavoidable due to the numerical effort involved in these simulations. Nevertheless, results from simulations such as presented here can help to shed light on stability properties of thin current sheets, such as found in the real magnetosphere.

A time step of an inverse electron plasma frequency $\omega_e \Delta t = 1$ is used. The ratio $\omega_e/\Omega_e$ is set to a numerical value of two. $12.5 \times 10^6$ ion and electron macro particles each are used in the simulation. We utilize an ion-electron mass ratio of $m_i/m_e = 100$, and will comment on the effect of a realistic mass ratio. The equilibrium particle distribution functions are chosen as shifted Maxwellians. The ion-electron temperature ratio is set to $T_e/T_i = 0.2$.

The magnetotail study initiates in a tail-like equilibrium of the class developed by (Birn and Schindler, 1983). Here the magnetic field is derived from a flux function

$$A = \ln\cosh(\nu(x)z/L) - \ln(\nu(x)/L). \tag{2}$$

The function $\nu(x)$ regulates the current sheet width dependence on the $x$ coordinate. For the purpose of this study, we adopt the following form

$$\nu = \left(1 + \frac{b_n x}{\gamma}\right)^{-\gamma} \tag{3}$$

which resembles the average properties of the magnetotail tailward of some 10–15 Earth radii (Birn and Schindler, 1983). Here the simulation region size is $x_{\max} = 60$, the exponent $\gamma = 0.6$, and the normal magnetic field component $B_z(x = 0, z = 0) = b_n = 0.05$. The plasma sheet half-width at the earthward edge of the simulation is two ion inertial lengths ($L = 2$), corresponding to some 1500 km for a plasma density of 0.1 cm$^{-3}$.

Runs without further modifications show this configuration to be tearing stable, at least for times less than about 400 ion cyclotron times, where no indication of instability could be seen. In order to study the impact of thin current sheet formation, however, we apply driving electric fields at the boundaries in the manner of Hesse *et al.* (1997), for times less than 20 ion cyclotron times. These driving electric fields increase the lobe magnetic field strength, and the flaring angle of the lobe field direction similar to what is found in actual observations (e.g., McPherron, 1979). As a result, previous simulations have shown the formation of thin current sheets (e.g., Hesse *et al.*, 1997), but none so far has been undertaken in a fully kinetic model with such large a mass ratio.

### 2.3 Onset of magnetic reconnection

The pressure in the center of the plasma sheet, and hence its gradient along $x$, are determined largely by the balance with the lobe magnetic pressure, which increases during the growth phase, driven by the external electric field. For a slowly driven evolution, force balance between the lobe and the plasma sheet should be maintained. This implies in particular that the radial pressure profile in the plasma sheet is given by the lobe magnetic pressure, which does not exhibit strong gradients in the radial direction. An additional increase of the current density inside the plasma sheet, as it is associated with the formation of a thin current sheet, hence must be accompanied by a reduction of $B_z$ and therefore by a change in the radial distribution of $B_z$. Otherwise, the radial plasma pressure gradient could not maintain force balance with the Lorentz force, given by the product $j_y B_z$. This scenario is illustrated in Fig. 1, which schematically depicts the formation of a thin current sheet within a thicker plasma sheet. External driving leads to a transition from an unperturbed state (top panel) to a state with an enhanced and localized current density (center panel). Now radial force balance requires a reduction of the magnetic field $B_z$ brought about by an expansion of the field lines in the regions of enhanced current density in the equatorial plane. Both of these effects are expected to destabilize the tail current sheet.

Figure 2 shows the evolution of the magnetic field and the current density (normalized to $B_0/(\mu_0 c/\omega_{pi})$) in the $x, z$ plane, demonstrating the formation of a thin current sheet and its subsequent breakup. Along with an increase in lobe magnetic field strength, the current density in the plasma sheet region increases strongly and disproportionally, in a localized region almost aligned with a magnetic flux tube. After $t = 80$, the current sheet becomes unstable and reconnection begins to operate, by X line formation, and a significant rearrangement of magnetic flux and current density is

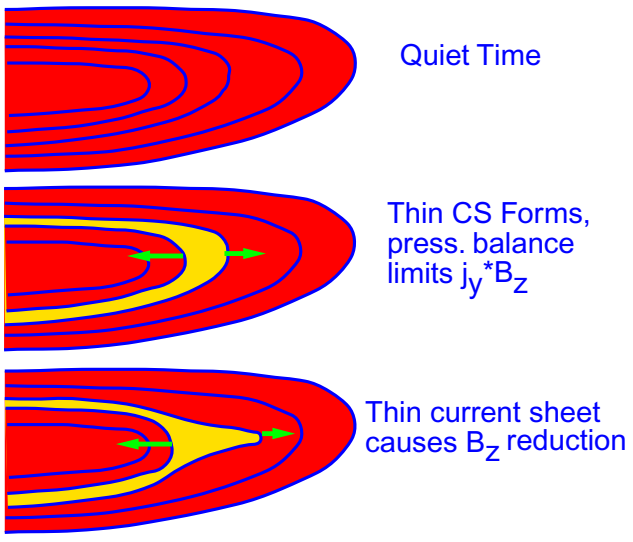


Fig. 1. Sketch of the formation of a thin current sheet (light) within the thicker plasma sheet (dark). The enhanced current density requires a reduction of the north-south magnetic field, with a weak divergent flow.

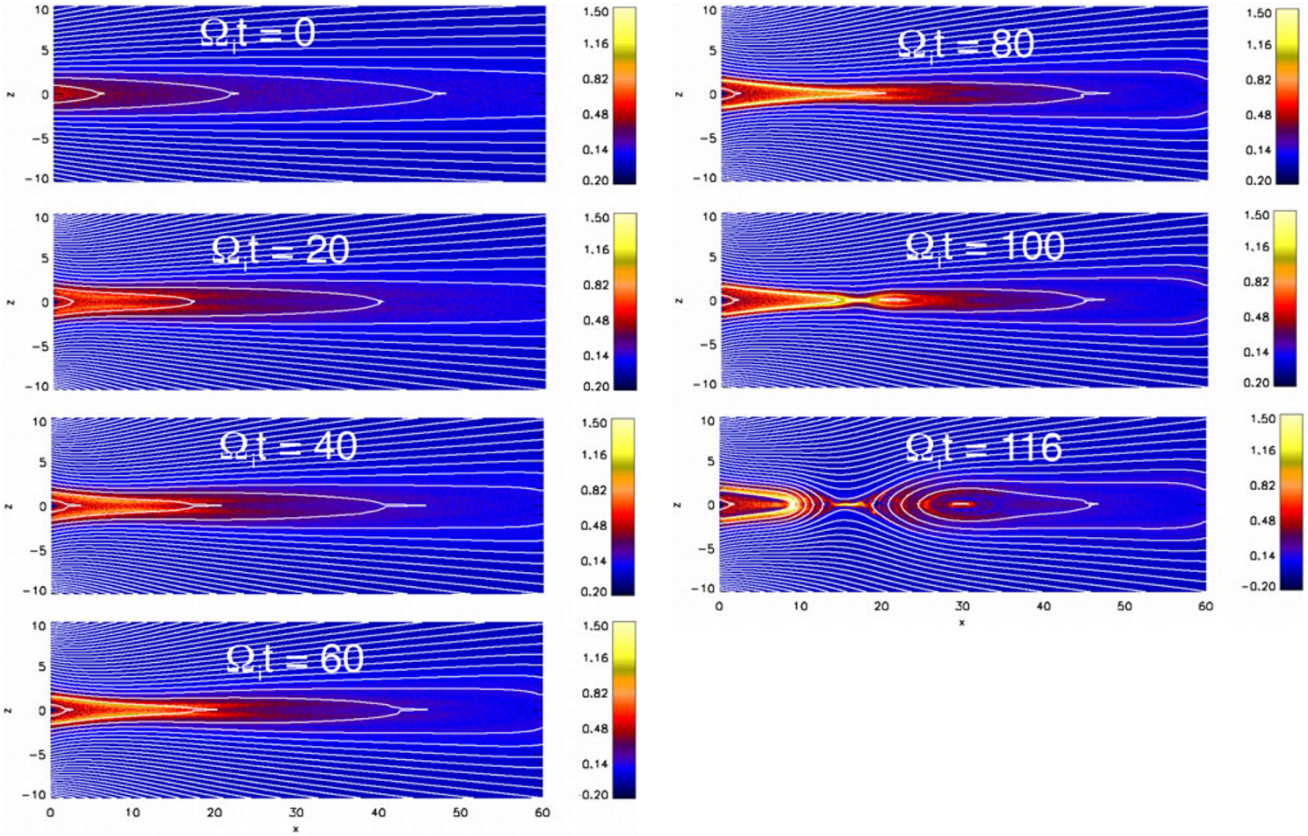


Fig. 2. Magnetic field evolution and current density (color coded) evolution. The figure shows the effects of driving, as well as strong changes brought about by magnetic reconnection.

evident. We will study the onset of the reconnection process below. At later times, the ion flow velocity in the central current sheet approaches the Alfvén speed.

The increase of magnetic flux through the $x = 0$ plane is evident in the graph of Fig. 3. The graph shows the effects of the driving boundary conditions, which generate a flux increase by about 65%. After termination of the driven phase ($t > 20$), the total magnetic flux remains constant, bearing evidence to the flux conservation quality of the simulation code. Figure 3 also shows the growth of the reconnected flux, defined as the negative integral of $B_z < 0$ over $x$ taken at the $x$ axis. The graph shows that reconnection initiates around $t = 90$, with a rapid, exponential growth following thereafter.

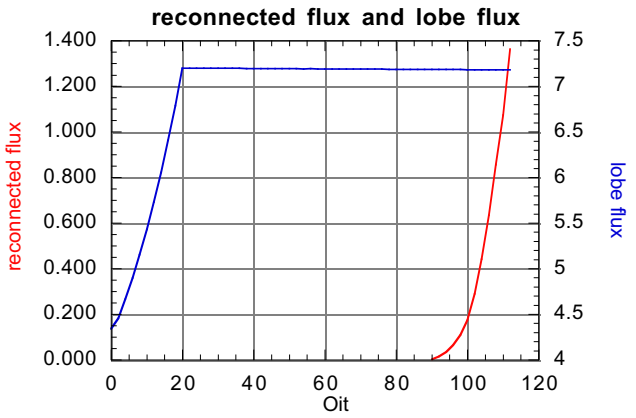


Fig. 3. Evolution of the total magnetic flux threading the $x = 0$, $z > 0$ half-axis, and of the newly reconnected flux threading the $x$ axis.

The evolution of the maximum current density in the $y$ direction is shown in Fig. 4. The figure demonstrates that the maximum current densities, taken both in the entire simulation box, and on the $x$ axis alone, exhibit an approximately linear growth, even after driving has ceased at $t = 20$. This growth behavior indicates a slow relaxation into a new equilibrium after the boundary conditions have been changed by the external driving. Given the distribution of particles on flux tubes, the system attempts to adjust to a new force balance subject to the new magnetic flux in the system and the new magnetic flux through the boundaries. Many numerical experiments of this relaxation process have been performed (e.g., Hesse *et al.*, 1997). Numerical model such as the one employed by Hesse *et al.* demonstrate that driving electric fields such as applied in the present study typically lead to the formation of a thin current sheet structure, initiating soon after driving ceases and evolving through the entire relaxation time. The latter is given by the interplay between wave propagation along the current sheet (i.e., in $x$), and across, i.e., in $z$. Assuming several wave bounce times are requires, the relaxation should complete in some 100–200 ion cyclotron periods. This process never does complete, however, because the thinning current sheet destabilizes a collisionless tearing instability.

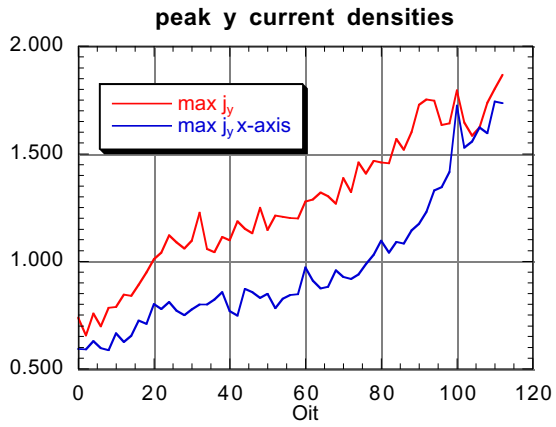


Fig. 4. Time evolution of the maximum of the current density component $j_y$ taken over the entire simulation domain, and on the $x$ axis alone. Both graphs exhibit an approximately linear increase with time.

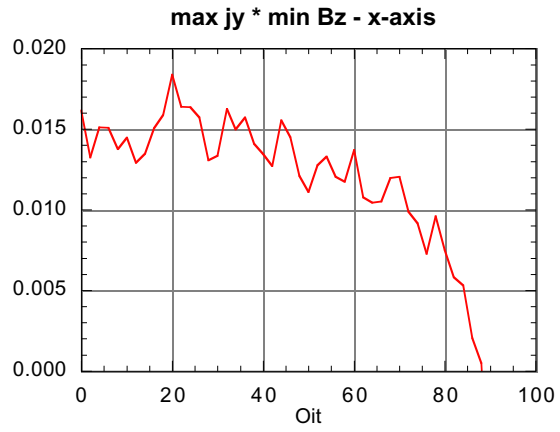


Fig. 5. Time evolution of the product of the maximum total current density in the $y$ direction, and the minimum of the normal magnetic field component $B_z$, all taken along the $x$ axis. The slow time dependence for $t < 80$ indicates an inverse proportionality of these two quantities, as expected from the qualitative arguments in the text.

A simple check of our assumption above relating $B_z$ reductions to $j_y$ enhancements is plotted in Fig. 5. The graph shows the time evolution of the product of the maximum of $j_y$, and the minimum of $B_z$, both taken on the $x$ axis. The graph shows until about $t \approx 80$ a moderate decrease. Clearly, the decrease of $B_{z,\min}$ overcompensates the increase of $j_{y,\max}$, which is likely to be due to using extreme rather than local values of $B_z$ and $J_y$. In any case, the absence of a strong increase indicates that our assumption above is at least qualitatively correct. After $t = 80$, other processes appear to take over, leading to a rapid reduction of the product despite the fact that the maximum current density continues to increase (see Fig. 4) until reconnection initiates.

The onset of magnetic reconnection in the present geometry requires that $B_z$ vanishes at the prospective reconnection site. Electron stabilization prevents this from occurring, unless a suitable diffusion mechanism becomes active. Thus the onset of magnetic reconnection requires a diffusive electric field $\mathbf{E}_D$ in the electron Ohm's law

$$\mathbf{E} + \mathbf{v}_e \times \mathbf{B} = \mathbf{E}_D \tag{4}$$

which we shall investigate in the following, for the time $\Omega_i t = 88$, just prior to $B_z < 0$ transition. In locations where $B$ becomes small, such that the $\mathbf{v}_e \times \mathbf{B}$-term becomes insignificant, this diffusive electric field has to be of sufficient magnitude to overcome the electric field.

A reduction in $B_z$, as evidenced in Fig. 6, is expected to lead to a destabilization (see Section 3). Figure 6 also displays the variation of the electron and ion current densities along the $x$ axis. Here we find strong enhancements of electron current density and only slight enhancements of ion current densities above their initial values, commensurate with earlier results (Hesse and Birn, 2000), and recent GEOTAIL observations (T. Mukai, private communications).

Previous investigations (e.g., Hesse *et al.*, 1999) have shown that the pressure-based contribution

$$E_{Dy} = -\frac{1}{ne}\left(\frac{\partial P_{xye}}{\partial x} + \frac{\partial P_{yze}}{\partial z}\right) \tag{5}$$

provides the dominant dissipation in slowly evolving systems. The present findings are consistent with that diffusion

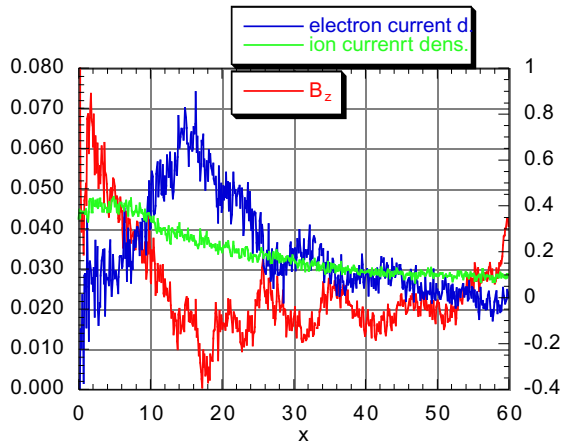


Fig. 6. Spatial variations of $B_z$, and the ion and electron current densities along the $x$ axis of the simulation box for $t = 88$. Here we find that the ion current density is slightly enhanced above the initial value, whereas the electron current density features major increases. At the location of electron current density maximum, the magnetic normal component $B_z$ appears strongly reduced.

mechanism. Inspection of the simulation results indicates that the most dominant contribution of (15) stems from the $x$ derivative of $P_{xye}$. In a situation with nonvanishing magnetic field, this term can be evaluated to an excellent approximation (e.g., Kuznetsova *et al.*, 1998)

$$P_{xye} \approx -\frac{p_e}{2\Omega_{ze}}\frac{\partial v_{xe}}{\partial x}. \tag{6}$$

Here $p_e$ denotes the isotropic part of the electron pressure tensor, $\Omega_{ze}$ the electron cyclotron frequency in the normal magnetic field, and $v_{xe}$ the $x$ component of the electron flow velocity.

The electron flow velocity is shown in Fig. 7, again for $t = 88$ and along the $x$ axis. Red color denotes the actual variation and black color a box-car smoothed version, which illustrates the variations more clearly. It is quite evident that

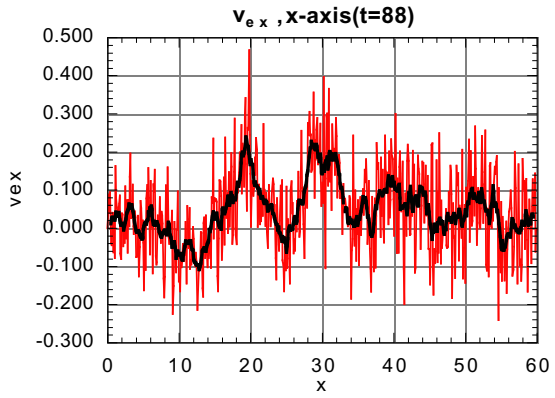


Fig. 7. Spatial variations of the electron flow velocity $v_{ez}$ along the $x$ axis of the simulation box for $t = 88$ (red) together with the result of as box car smoothing (black). The latter is shown to illustrate the struture near the site of interest. Here we find the existence of strong velocity gradients which support the formation of electron pressure anisotropies.

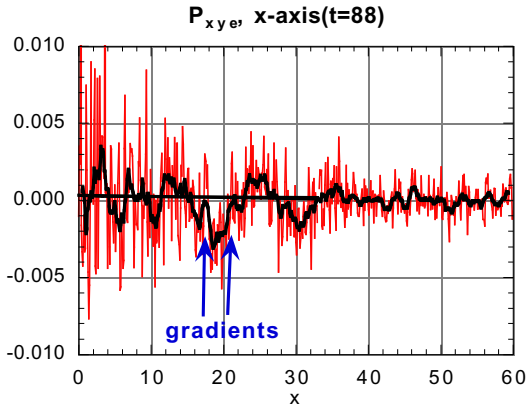


Fig. 8. Spatial variations of the (nongyrotropic) electron pressure tensor component $P_{xye}$ along the $x$ axis of the simulation box for $t = 88$ (red) together with the result of as box car smoothing (black). The latter is shown to illustrate the struture near the site of interest. Here we find gradients at the site of reduced $B_z$ which provide a dissipative electric field.

the $x$ derivative of $v_{ex}$ reverses sign at about $x = 18$, the site of strong $B_z$ reduction. As a result, Eq. (6) indicates that $P_{xye}$ should exhibit a finite gradient at $x = 18$, leading to a finite value of the electric field (5).

The pressure tensor component does indeed feature the needed gradient (see (5)), as can be seen from the graph of Fig. 8, which displays the actual variation of $P_{xye}$ (red) together with a smoothed graph (black). The plotted variation of $P_{xye}$ along $x$ at $t = 88$ clearly exhibits a negative gradient around the site of the $B_z = 0$ transition, giving rise to a positive value of $E_{Dy}$, which roughly agrees with the required value.

One might wonder how the system can maintain such large nongyrotropies of the electron pressure tensor in the presence of a normal component of the magnetic field. One answer to this question is provided by the velocity gradient evident in Fig. 7. The other is related to the local electron Larmor radius, which can get rather large (for the present mass ratio) and the reduced normal magnetic field. The electron Larmor radius, based on the local magnetic field and the local electron temperature, is plotted logarithmically in Fig. 9. Here we find strong enhancements at the site of $B_z$ reduction, where the local Larmor radius exceeds the system's dimensions. Clearly, electrons are strongly demagnetized in this situation. As a result, distribution function are not a priori expected to be gyrotropic, and the anisotropies seen in Fig. 8 can result.

We note that our simulation exhibits a large but still unrealistic electron-to-ion mass ratio. In order to estimate the effects of a realistic mass ratio, we scale the expression (6) for the electron pressure anisotropy

$$P_{xye} \approx -\frac{p_e}{2\Omega_{ze}} \frac{\partial v_{xe}}{\partial x} \sim \frac{m_e}{B_z} \qquad (7)$$

Thus the same amount of electron pressure anisotropy for realistic mass ratio requires a $B_z$ reduction by a factor of about $r = 18$. Going back to the argument above, the inverse proportionality of $B_z$ and $j_y$ would then require a $j_y$ enhancement by a factor $r = 18$. While this might sound unreasonable at first, we point out that the current density in our model was enhanced by a factor of less than three before a diffusive process took over. Also, simulations which do not feature full electron dynamics, both using MHD (Birn *et al.*, 1998), and hybrid simulations (Hesse *et al.*, 1995) consistently show that current densities can increase by factors of ten or more for reasonable driving boundary conditions. We therefore expect that current sheets will get thin enough, and current densities strong enough, to facilitate the onset of magnetic reconnection even for realistic electron mass, i.e. in the real magnetotail.

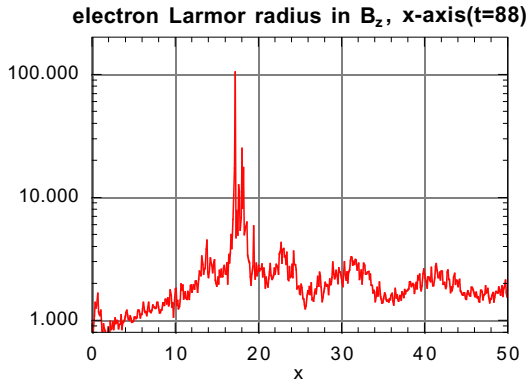


Fig. 9. Spatial variations of the thermal electron Larmor radius along the $x$ axis of the simulation box for $t = 88$. Here we find very large Lamor radii around the site of reduced $B_z$ which allow the formation of significant pressure anisotropies.

Our results, presented in the present paper, are based on a two-dimensional model. Therefore, the present model is incapable of addressing the often-observed spatial localization of magnetic reconnection in the direction across the magnetotail (e.g., Angelopoulos *et al.*, 1992). On the other hand, extending the model to three dimensions increases substantially the amount of dissipative modes (by all modes with finite wave number $k_y$), so that a more unstable behavior could result. Therefore, it is, at the present time, unclear what will be found in a three-dimensional model. Our re-

sults do suggest, however, that thin current sheet formation can destabilize collisionless tearing in an otherwise stable magnetotail configuration.

## 3. Linear Stability

The simulation results described above suggest that an instability arises as the electrons become sufficiently nongyrotropic. To complement the simulation results, here we briefly discuss this problem in an analytical context using the variational principle of two-dimensional collisionless plasmas (Schindler *et al.*, 1973; Goldstein and Schindler, 1982). For translational invariance with respect to one cartesian coordinate ($y$) and for equilibrium distribution functions monotonically decreasing with energy a potential energy $V$ can be defined, such that its second variation $V_2(A_1)$ with respect to the linear perturbation $A_1$ of the magnetic flux function provides rigorous information on stability. Here, $V_2$ plays a role similar to that of the second derivative of potential energy of a Hamiltonian system with one degree of freedom. The fact that the plasma system has infinitely many degrees of freedom is reflected by $V_2(A_1)$ being a functional (of the function $A_1(x, z)$) rather than a function of a variable. Although the theoretical formulation of this approach is available for nearly 30 years, the information that one has extracted from it has been rather limited. This may be explained by the complicated structure of $V_2(A_1)$, which involves nonlocal features manifested by phase space averages. An additional complication is the quasi-neutrality condition which poses a constraint to the variational procedure in the form of an integral equation. Here we show how a simplified analysis can provide information about the role of nongyrotropic electrons in thin current sheets.

The functional $V_2$ has the following general form,

$$V_2(A_1) = \frac{1}{2}\int\left(\frac{(\nabla A_1)^2}{\mu_0} - \frac{dj_y(A)}{dA}A_1^2 + Q(A_1)\right)dxdz$$

where $j_y(A)$ is the equilibrium current density (depending on the equilibrium flux function $A$ only) and $Q(A_1)$ a positive term containing the phase space averages, with $A_1$ denoting the flux function describing the perturbation electric field. It turns out that positiveness of $V_2(A_1)$ is necessary and sufficient for stability with respect to modes with the same symmetry as the equilibrium, i.e. independence of $y$. Obviously, instability can arise at most from the second term ('driving term') in the integrand. In fact, that term is typically negative in current sheets and describes the attractive interaction between parallel currents.

The limit of small electron gyroradii is appropriately described by simply fixing the number of electrons in each magnetic flux tube. The corresponding form of $Q$, here denoted as $Q_0$, takes the form (Pellat *et al.*, 1991; Quest *et al.*, 1996),

$$Q_0 = p\left(\frac{1}{V(A)}\frac{d}{dA}\int_A A_1\frac{ds}{B}\right)^2$$

where $p$ is the equilibrium pressure, and $s$ the arc-length and $V$ the flux tube volume on field lines. As Pellat *et al.* have shown , a small normal component $B_n$ leads to large values of $Q_0$, which scales as $1/B_n$ (see also Quest *et al.*, 1996). Since the other terms in $V_2$ are of order 1 (in $B_n$) the system is stable. This confirms that an instability requires nongyrotropic electrons.

We can make this statement more quantitative in the following way. It is convenient to measure electron gyrotropy by the parameter $\zeta = k\rho_n = \kappa\rho_0$, where $k$ is the wave number of the test mode with respect to the $x$-coordinate, $\rho_n$ and $\rho_0$ being the electron gyro-radius in the normal field $B_n$ at $z = 0$ and for a typical value of the asymptotic field $B_0$, respectively, such that $\kappa = k/b_n$ with $b_n = B_n/B_0$. It is possible to identify the leading term in $Q$ that goes to $Q_0$ for vanishing $\zeta$ in the exact form of $V_2$. Comparing that term with the driving term for different values of $\zeta$ we can find a $\zeta$-range for which the two terms typically become comparable. Roughly, this would be the range, where an instability can be expected to occur. Thus, we are interested in the ratio $K$ of the integrated stabilizing term $\int Q dxdz$ and the magnitude of the integrated driving term $|\int \frac{dj_y(A)}{dA}A_1^2 dxdz|$. We computed this ratio for a fixed typical test function $A_1$, using a simplified model of $Q$, which, however, becomes correct in the limits of large and small values of $\zeta$. Details will soon be published elsewhere. Figure 10 shows the results of such a study, where $\log K$ is plotted as a function of $\log\zeta$ for three values of $\kappa$. As expected, in the limit of small $\zeta$, $K$ approaches the large values that one finds by using $Q_0$ instead of $Q$ (horizontal lines). As $\zeta$ increases $K$ decreases and roughly for $\zeta$ near 1 the ratio $K$ passes through 1, such that one can expect an instability to arise. In fact, for large $\zeta$ the $Q$-term becomes small and $V_2$ reduces to the 'Schroedinger'-form of $V_2$, which is known to assume negative values associated with the tearing instability (e.g., Schindler and Birn, 1978).

These findings support our interpretation of the simulation results. From Fig. 6 we conclude that in the onset region near $x = 18$ (see Fig. 9) a clearly visible half-wave has an extent of about 25, corresponding to $k \approx 0.13$. Here the half-wave is defined by the overall variation of $B_z$ along $x$, ranging from $x = 0$ to approximately $x = 25$. Smaller wavelengths are also found but we do not believe that they

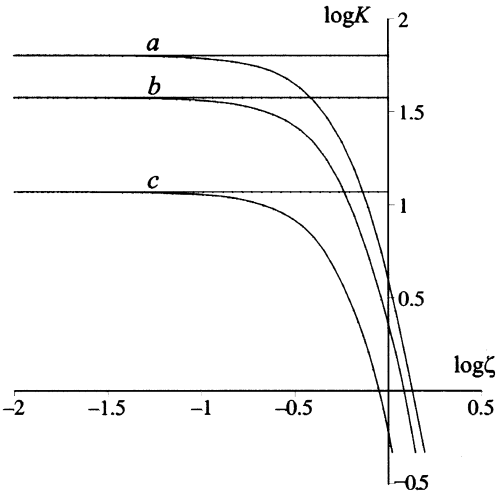


Fig. 10. Here $\log K$ is plotted versus $\log\zeta$. The curves $a$, $b$, $c$ correspond to $\kappa = 5\pi, 3\pi, \pi$, respectively. The horizontal lines represent the asymptotic values corresponding to the choice $Q = Q_0$.

contribute to the growth of the tearing instability. The initial value of $\rho_n$ can be estimated from the equilibrium quantities. Using approximate pressure balance one finds $\rho_n \approx 1.0$. Thus, the initial value of $\zeta$ becomes $\zeta_0 \approx 0.13$. At $t = 88$, $\rho_n$ has risen to a value of, say 5, an estimated average value that would seem consistent with Fig. 9. This gives the values 0.65 and 13 for $\zeta$ and $\kappa$, respectively. Applying these numbers to Fig. 10 indicates that indeed during the driven phase (before $t = 88$) the value of $Q$ strongly decays due to increasing electron nongyrotropy. Thus, from the model the onset of the instability is expected roughly at the observed time.

Clearly, precise quantitative coincidence cannot be expected because of differences in the configuration and the simplifications of the model. More reliable result must come from a full minimization procedure including the charge neutrality condition. Also, more investigations are necessary to find out whether the role of $\zeta$ as the single relevant onset parameter also applies to parameter regimes wider than that studied here.

## 4. Summary

In this paper, we presented an investigation of kinetic processes in the magnetotail plasma sheet, which give rise to the onset of magnetic reconnection. All simulation studies presented here are based on the application of our self-consistent fully electromagnetic particle-in-cell simulation code, albeit in a simpler, 2.5-dimensional geometry.

Like the natural procession of events in a magnetospheric substorm, our first focus was on the formation of thin current sheets during the substorm growth phase. Here we found, consistent with earlier analyses, that thin current sheets form if a driving electric field is applied to a magnetotail model, similar to what would be expected for the effects of the solar wind.

We found the formation of a strong, highly localized current density enhancement, which is provided by the electrons. This current density enhancement was accompanied by a reduction in the north-south magnetic field component $B_z$ and of the current sheet thickness. Both effects are expected to destabilize the current sheet, and eventually initiate reconnection.

The simulation indeed led to the onset of reconnection and the typical features commonly associated with substorm expansion, within the limits of the 2.5-dimensional model. We then conducted a study of the diffusive electric field in the spatial region which becomes the locus of the X point in the subsequent evolution. We found the existence of a weak, divergent electron flow in the $x$ direction, as required for the reduction of $B_z$. Such flows, together with gradients in the electron cyclotron frequency, can give rise to electron pressure anisotropies, and thereby generate diffusive electric fields. The existence of these pressure anisotropies was verified by direct inspection of the simulation results, and motivated by the magnitude of the local electron Larmor radius. Thus we concluded that electron pressure based dissipation is likely responsible for the onset of magnetic reconnection, as well as for its operation thereafter.

The picture of an instability arising at a sufficiently high level of electron nongyrotropy was also tested with the help of the energy principle of two-dimensional collisionless plasmas using a simplified analysis. The results give full support to that picture.

There still are a number of open questions associated with this result. First, one might wonder whether current sheets can become thin enough if a realistic ion/electron mass ratio, rather than $m_i/m_e = 100$, were employed. While computational capabilities presently prohibit answering this question, we refer to ideal MHD simulations, which showed that current density enhancements of some factor of ten can be expected for reasonable electric field driving, and in the absence of dissipation (Birn *et al.*, 1998). Therefore, we are led to conclude that, in reality, the current sheet would just continue to thin until a dissipation mechanisms would be excited, initiating magnetic reconnection. Based on the present results, we would require the current sheet to be strong enough to reduce $B_z$ to the point where the local electron Larmor radius exceeds the gradient scale length of the reduced $B_z$.

Thus, a reduction of $B_z$ associated with thin current sheet formation plays a critical role in destabilizing collisionless tearing, and in enabling magnetic reconnection, even in the absence of other kinetic processes. Collisionless tearing and magnetic reconnection thus remain a crucial ingredient in magnetospheric dynamics, a fact which is strongly supported by the clear evidence of magnetic reconnection provided by GEOTAIL observations (e.g., Nagai *et al.*, 1998).

**Acknowledgments.** This work was supported by NASA's Sun-Earth-Connection Theory and Supporting Research and Technology Programs.

## References

Angelopoulos, V., W. Baumjohann, C. F. Kennel, F. V. Coroniti, M. G. Kivelson, R. Pellat, R. J. Walker, H. Lühr, and G. Paschmann, Bursty bulk flows in the inner central plasma sheet, *J. Geophys. Res.*, **97**, 4027, 1992.

Antiochos, S. K., C. R. DeVore, and J. A. Klimchuk, A model for solar coronal mass ejections, *Astrophys. J.*, **510**, 485, 1999.

Atkinson, G., Field-line merging and slippage, *Geophys. Res. Lett.*, **5**, 465, 1978.

Birn, J. and K. Schindler, Self-consistent theory of three-dimensional convection in the geomagnetic tail, *J. Geophys. Res.*, **88**, 6969, 1983.

Birn, J., M. Hesse, and K. Schindler, Formation of thin current sheets in space plasmas, *J. Geophys. Res.*, **103**, 6843, 1998.

Birn, J., J. F. Drake, M. A. Shay, B. N. Rogers, R. E. Denton, M. Hesse, M. M. Kuznetsova, Z. W. Ma, A. Bhattacharjee, A. Otto, and P. L. Pritchett, GEM magnetic reconnection challenge, *J. Geophys. Res.*, **106**, 3715, 2001.

Brueckner, G. E., Global Coronal Disturbances as the Source for the Low Latitude Solar Wind, Transactions AGU, SH72B-05, 1996.

Cai, H. J. and L. C. Lee, The generalized Ohm's law in collisionless magnetic reconnection, *Phys. Plasmas*, **4**, 509, 1997.

Cargill, P. A. and J. A. Klimchuk, A nanoflare explanation for the heating of coronal loops observed by Yohkoh, *Astrophys. J.*, **478**, 799, 1997.

Goldstein, H. and K. Schindler, Large-scale collision-free instability of two-dimensional plasma sheets, *Phys. Rev. Lett.*, **48**, 1468, 1982.

Gosling, J. T., J. Birn, and M. Hesse, Three-dimensional magnetic reconnection and the magnetic topology of coronal mass ejection events, *Geophys. Res. Lett.*, **22**, 869, 1995.

Haerendel, G., On the potential role of field-aligned currents in solar physics, Proceedings of 21st ESLAB Symposium, Bolkesjø, Norway, European Space Agency, Paris, 1987.

Hesse, M. and J. Birn, Near- and mid-tail current flow during substorms: Small- and large-scale aspects of current disruption, in *Magnetospheric Currents*, Geophys. Monogr. Ser., edited by S. Ohtani, R. Lysak, and M. Hesse, p. 295, AGU, Washington, D.C., 2000.

Hesse, M. and D. Winske, Electron dissipation in collisionless magnetic

reconnection, *J. Geophys. Res.*, **103**, 26479, 1998.
Hesse, M., D. Winske, and M. M. Kuznetsova, Hybrid Modeling of collisionless reconnection in two-dimensional current sheets: Simulations, *J. Geophys. Res.*, **100**, 21815, 1995.
Hesse, M., D. Winske, and J. Birn, On the ion scale structure of thin current sheets in the magnetotail, *Phys. Scr.*, **T74**, 63, 1997.
Hesse, M., K. Schindler, J. Birn, and M. Kuznetsova, The diffusion region in collisionless magnetic reconnection, *Phys. Plasmas*, **6**, 1781, 1999.
Hewett, D. W., G. E. Frances, and C. E. Max, New regimes of magnetic reconnection in collisionless plasma, *Phys. Rev. Lett.*, **61**, 893, 1988.
Horiuchi, R. and T. Sato, Particle simulation study of driven magnetic reconnection in a collisionless plasma, *Phys. Plasmas*, **1**, 3587, 1994.
Horiuchi, R. and T. Sato, Particle simulation study of collisionless driven reconnection in a sheared magnetic field, *Phys. Plasmas*, **4**, 277, 1997.
Krauss-Varban, D. and N. Omidi, Large-scale hybrid simulations of the magnetotail during reconnection, *Geophys. Res. Lett.*, **22**, 3271, 1995.
Kuznetsova, M. M., M. Hesse, and D. Winske, Hybrid Modeling of the tearing instability in collisionless two-dimensional current sheets: Linear Theory, *J. Geophys. Res.*, **100**, 21827, 1995.
Kuznetsova, M., M. Hesse, and D. Winske, Kinetic quasi-viscous and bulk flow inertia effects in collisionless magnetotail reconnection, *J. Geophys. Res.*, **103**, 199, 1998.
Langdon, A. B., On enforcing Gauss' law in electromagnetic particle-in-cell codes, *Comp. Phys. Comm.*, **70**, 447, 1992.
Lin, Y. and D. W. Swift, A two-dimensional hybrid simulation of the magnetotail reconnection layer, *J. Geophys. Res.*, **101**, 19859, 1996.
Lottermoser, R.-F., M. Scholer, and A. P. Matthews, Ion kinetic effects in magnetic reconnection: Hybrid simulations, *J. Geophys. Res.*, **103**, 4547, 1998.
McPherron, R. L., Magnetospheric substorms, *Rev. Geophys.*, **17**, 657, 1979.
Nagai, T., *et al.*, Structure and dynamics of magnetic reconnection for substorm onsets with Geotail observations, *J. Geophys. Res.*, **103**, 4419, 1998.
Pellat, R., F. Coroniti, and P. Pritchett, Does ion tearing exist?, *Geophys. Res. Lett.*, **18**, 143, 1991.
Paschmann, G., *et al.*, Plasma acceleration at the earth's magnetopause: Evidence for reconnection, *Nature*, **282**, 243, 1979.
Priest, E. R., Magnetic reconnection at the sun, in *Magnetic Reconnection in Space and Laboratory Plasmas*, Geophys. Monogr. Ser., vol. 30, edited by E. W. Hones, p. 63, AGU, Washington, D.C., 1984.
Priest, E. R. and T. G. Forbes, Steady magnetic reconnection in three dimensions, *Solar Phys.*, **119**, 211, 1989.
Pritchett, P. L., Effect of electron dynamics on collisionless reconnection in two-dimensional magnetotail equilibria, *J. Geophys. Res.*, **99**, 5935, 1994.
Quest, K. B., H. Karimabadi, and M. Brittnacher, Consequences of particle conservation along a flux surface for magnetotail tearing, *J. Geophys. Res.*, **101**, 179, 1996.
Schindler, K. and J. Birn, Magnetospheric physics, *Phys. Reports*, **47**, 109, 1978.
Schindler, K., D. Pfirsch, and H. Wobig, Stability of two-dimensional collison-free plasmas, *Plasma Phys.*, **15**, 1165, 1973.
Shay, M. A., J. F. Drake, R. E. Denton, and D. Biskamp, Structure of the dissipation region during collisionless magnetic reconnection, *J. Geophys. Res.*, **103**, 9165, 1998a.
Shay, M. A. and J. F. Drake, The role of electron dissipation on the rate of collisionless magnetic reconnection, *Geophys. Res. Lett.*, **25**, 3759, 1998b.
Sonnerup, B. U. Ö., *et al.*, Evidence for magnetic field reconnection at the earth's magnetopause, *J. Geophys. Res.*, **86**, 10049, 1981.
Tanaka, M., Macro-particle simulations of collisionless magnetic reconnection, *Phys. Plasmas*, **2**, 2920, 1995a.
Tanaka, M., The macro-em particle simulation method and a study of collisionless magnetic reconnection, *Comp. Phys. Comm.*, **87**, 117, 1995b.
Vasyliunas, V. M., Theoretical models of magnetic field line merging, 1, *Rev. Geophys.*, **13**, 303, 1975.
Villasenor, J. and O. Buneman, Rigorous charge conservation for local electromagnetic field solvers, *Comp. Phys. Comm.*, **69**, 306, 1992.

M. Hesse (e-mail: michael.hesse@gsfc.nasa.gov) and K. Schindler